Covalent functionalization of boron nitride nanotubes via reduction chemistry

Shin, Homin; Guan, Jingwen; Zgierski, Marek Z.; Kim, Keun S.; Kingston, Christopher T.; Simard, Benoit

Publisher's version / Version de l'éditeur:
https://doi.org/10.1021/acsnano.5b06523
ACS Nano, 9, 12, pp. 12573-12582, 2015-11-18

Covalent Functionalization of Boron Nitride Nanotubes *via* Reduction Chemistry

Homin Shin,* Jingwen Guan, Marek Z. Zgierski, Keun Su Kim, Christopher T. Kingston, and Benoit Simard

Security and Disruptive Technologies Portfolio, Emerging Technologies Division, National Research Council Canada, Ottawa, Ontario K1A 0R6, Canada

ABSTRACT Boron nitride nanotubes (BNNTs) exhibit a range of properties that hold great potential for many fields of science and technology; however, they have inherently low chemical reactivity, making functionalization for specific applications difficult. Here we propose that covalent functionalization of BNNTs *via* reduction chemistry could be a highly promising and viable strategy. Through density functional theory calculations of the electron affinity of BNNTs and their binding energies with various radicals, we reveal that their chemical reactivity can be significantly enhanced *via* reducing the nanotubes (*i.e.*, negatively charging). For example, a 5.5-fold enhancement in reactivity of reduced BNNTs toward NH_2 radicals was predicted relative to their neutral counterparts. The localization characteristics of the BNNT π electron system lead the excess electrons to fill the empty p orbitals of boron sites, which promote covalent bond formation with an unpaired electron from a radical molecule. In support of our theoretical findings, we also experimentally investigated the covalent alkylation of BNNTs *via* reduction chemistry using 1-bromohexane. The thermogravimetric measurements showed a considerable weight loss (12−14%) only for samples alkylated using reduced BNNTs, suggesting their significantly improved reactivity over neutral BNNTs. This finding will provide an insight in developing an effective route to chemical functionalization of BNNTs.

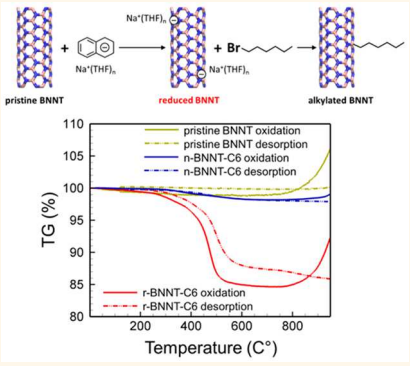

KEYWORDS: boron nitride nanotubes · covalent functionalization · reduction · density functional theory

Boron nitride nanotubes (BNNTs) consist of seamless cylinders of alternating boron and nitrogen atoms in a hexagonal BN bonding network.[1,2] Since their first synthesis in 1995,[1] BNNTs have been considered as revolutionary materials due to their unique properties, which are as compelling as those of carbon nanotubes (CNTs). Despite their structural similarity to CNTs, BNNTs also exhibit a range of physical and chemical properties distinct from CNTs, which are mainly attributed to the partial ionic bonding character of BN. For example, the mixed ionic and covalent bonding nature of BNNTs results in their wide band gaps, around 6.0 eV independent of diameter and chirality. Figure 1 illustrates the calculated valence electron density distribution of a (6,6) CNT and BNNT. The valence charges of a CNT are equally distributed around C atoms, indicating a strong covalent C−C bond network as well as the delocalized electrons, while the bonding electrons of BNNT are more concentrated around N atoms with an asymmetric charge distribution, owing to the difference in the electronegativity between B (2.04) and N (3.04) atoms. Consequently, the electron delocalization on BNNTs is weaker than that on CNTs, but sufficient to maintain planar sp^2 hybridization. In this paper, we explore how such weaker delocalization of π electrons in BNNTs can be beneficial in their covalent functionalization with radical molecules, particularly when tube surfaces are reduced.

Very recently, notable advances in the large-scale production of high-quality and high-purity BNNTs have been achieved by laser and thermal plasma processes.[3−5] These developments promise to stimulate greater research on the applications of BNNTs, such as nanocomposites,[6] which have not been widely explored due to the previously limited accessibility to sufficient quantities of material. To be successful, methods for dispersing and integrating BNNTs into solvents and different matrices will be required, for which chemical modification of BNNT surfaces is crucial. A range

* Address correspondence to Homin.Shin@nrc-cnrc.gc.ca.

Received for review October 16, 2015 and accepted November 18, 2015.

Published online November 18, 2015
10.1021/acsnano.5b06523

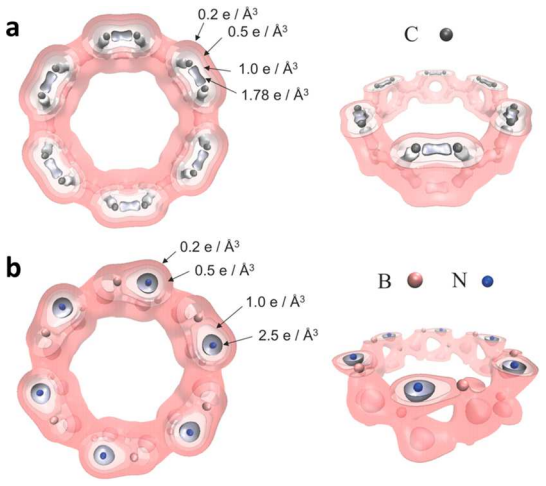

Figure 1. Total valence electron distributions of a (6,6) CNT (a) and BNNT (b) at various isovalues of charge densities as indicated. The tube models represent one unit cell of (6,6) nanotubes with 24 atoms.

of functionalization methods for BNNTs have been explored, from utilizing Lewis acid−base interactions[7,8] to noncovalent functionalization *via* polymer wrapping;[9−11] however, the low reactivity of BNNTs often makes their surface functionalization difficult. The main challenge in promoting the chemical reactivity on BNNT surfaces is largely attributed to the lack of covalent chemistry of the empty orbital on B sites. There have been few reports to date for direct covalent functionalization of BNNTs,[12] although it has been realized on the surfaces of planar hexagonal boron nitride (h-BN) sheets by generating free radical species, such as oxygen radicals or nitrenes, *via* thermolysis.[13−15]

In this paper, we propose a promising route toward covalent functionalization of BNNTs through reduction of the nanotubes (*i.e.*, charging with negative charges) followed by reactions with free radicals. For CNTs, various reduction methods employing dissolved alkali metals have already been applied to promote both dispersion and functionalization. Solutions of alkali metal naphthalide salts in tetrahydrofuran (THF) have been shown to be very efficient at promoting spontaneous dispersion of SWCNTs[16,17] as well as greatly increasing their chemical reactivity.[18,19] Using alkali metals dissolved in liquid ammonia is another method of generating solvated electrons that transfer to the CNTs to produce radical CNT anions.[20,21] This route has been employed for functionalization with a series of alkyl and aryl groups. Several extended works have demonstrated the efficiency and scalability of reduction functionalization on CNTs,[22−27] yet the similar approaches have yet to be investigated for the functionalization of BNNTs, neither by theory nor experiment.

Here we demonstrate through density functional theory (DFT) calculations that reduced BNNTs are stable species, particularly at small diameters, by evaluating electron affinity (EA), which is the key element to estimate the stability of BNNT radical anions. Such electron-accepting properties of nanotubes have rarely been investigated. To our knowledge, no prior theoretical or experimental studies on the EA of BNNTs have been reported, and only a few DFT calculations have been carried out for CNTs.[28−30] Moreover, our theoretical studies reveal that the chemical reactivity of BNNTs toward various radicals, such as $^{\bullet}CH_3$, $^{\bullet}NH_2$, $^{\bullet}OH$, and $^{\bullet}NH$, can be significantly improved when they are negatively charged, which has not been reported for their carbon counterparts. Our finding of significant improvement in the BNNT's capability of adsorbing radical molecules upon tube surface reduction suggests that reduced BNNTs can serve as effective intermediates in further facilitating covalent functionalization. We discuss that the reactivity enhancement of reduced BNNTs is due to their localization characteristics of the π electron system and is also affected by the detailed electronic structures of radical species, which could provide useful guidelines in the development of effective covalent functionalization schemes for BNNTs. Lastly, we briefly demonstrate the covalent alkylation of BNNTs *via* a reduction reaction using 1-bromohexane in support of our theoretical findings.

RESULTS AND DISCUSSION

Electron Affinities. In previous studies,[28−30] the EA was defined as the energy gain upon adding an electron to a nanotube segment, mostly in the form of finite clusters with or without hydrogen atoms on the edges. Here, we extend this *gas phase* definition of EAs[31] to infinitely long nanotube systems; periodic boundary conditions are applied, and one extra electron is inserted per supercell. Different cell lengths along the tube axis are also considered in order to allow varying charge density per tube. Then, we evaluate the EA for a nanotube (NT) supercell model containing N atoms as the energy difference between a neutral tube and its negatively charged counterpart:

$$\mathrm{EA} = E_{\mathrm{tot}}(\mathrm{NT}) - E_{\mathrm{tot}}(\mathrm{NT}^{-})$$

where $E_{\mathrm{tot}}(\mathrm{NT})$ and $E_{\mathrm{tot}}(\mathrm{NT}^{-})$ are the total ground-state energies of the optimized neutral and charged nanotube configurations, respectively. Thus, the calculated EAs are interpreted as the measure of energy gain or loss by negatively charging a nanotube with a charge density of $\rho = -1/N$ (e/atom). Note that we assume nanotubes maintain on average a constant charge density of additional electrons throughout the entire tube length. This approach allows us not only to compare the trend of EAs among different types and structures of nanotubes (within a single theoretical framework) but also to explore a range of charge density on the tube surface by varying supercell lengths or changing the number of extra electrons.

The tube structures extensively examined in this study are armchair (5,5) and zigzag (5,0) nanotubes.

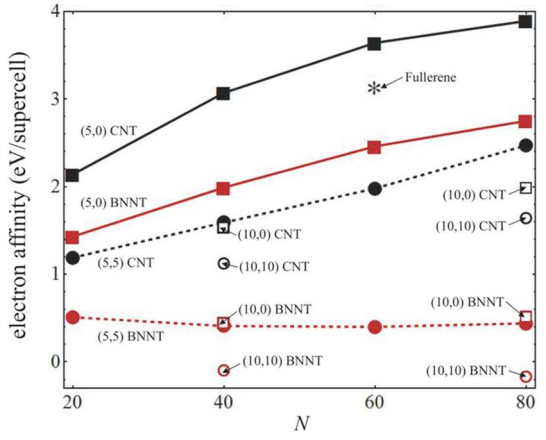

Figure 2. Electron affinities (eV/supercell) with respect to the various model supercell sizes containing *N* atoms (or the inverse of charge density $\rho = -1/N$) are plotted for CNTs and BNNTs. Various NT structures (5,5), (5,0), (10,10), and (10,0) are considered. We also include the EA of fullerene (*) obtained using the same calculation scheme.

We carried out the EA calculations for supercells containing N = 20, 40, 60, and 80, which correspond to 1, 2, 3, and 4 unit cells, respectively. Hence, the extra electron density ranges from $\rho = -1/20$ to $\rho = -1/80$ (*e*/atom), which fall into the experimental ranges of the exact charge: C ratios, for example, from 1:10 to 1:370, obtained from a reduction reaction of CNTs in THF with a K/naphthalene salt.[17] In order to investigate the effect of tube diameters on the EAs, we also examined (10,10) and (10,0) nanotube models with supercells of N = 40 and 80, which correspond to 1 and 2 unit cells, respectively.

The EA calculation results are summarized in Figure 2. As a benchmark point, we also calculated the EA of fullerene, which is found to be 3.16 eV, close to the value of 2.95 eV estimated in the literature;[28] both of these theoretical estimations are higher than the experimental EA value of fullerene, which is 2.69 eV.[32] Most of the EAs calculated for CNTs and BNNTs in this study are found to be positive, which implies that free electron transfer to the tube surfaces is favorable for both nanotubes, and, hence, the reduced nanotube anions are stable species. Note that, however, the EAs of (10,10) BNNTs are estimated to be slightly negative, with values of −0.10 eV for N = 40 and −0.17 eV for N = 80. The results predict that the EAs strongly depend on the constituent elements of the nanotubes (C or BN), nanotube structures (armchair or zigzag), nanotube diameters, and charge density (or supercell length). When the same nanotube structure is considered, CNTs are always predicted to have a larger energy gain than BNNTs, for the same charge density. For instance, the released energy per supercell by charging (5,5) nanotubes with a charge density of $\rho = -1/60$ (*e*/atom) is estimated as 0.40 eV for a BNNT and 1.98 eV for a CNT.

We also observed a trend that the EA increases as the nanotube diameter decreases for both zigzag and armchair structures; the EA for a (5,0) (or (5,5)) nanotube is larger than that of a (10,0) (or (10,10)) nanotube for the same kind of nanotube. A similar curvature-dependent trend has been observed for various carbon nanomaterials in the literature (*e.g.*, EA($CNT_{(5,0)}$) > EA(fullerene) > EA($CNT_{(5,5)}$)).[28] This finding implies that the curvature-induced π orbital misalignment results in an enhanced reactivity toward extra electrons, whereby nanotubes release strain energy associated with high curvature by reduction.[33] Such curvature dependency of the EA seems to be generic for both fully (CNTs) and partially (BNNTs) delocalized π electron systems. The observation suggests that using small-diameter nanotubes is expected to be more effective for tube reduction and also for facilitating their functionalization with subsequent chemical reactions.

As noted, the present EA calculations suggest that, in the gas phase, CNTs have a stronger tendency to accept electrons than the same structural BNNTs. The affinity for CNTs to accept negative charges has been explored through recent experiments of the reduction of CNTs with alkali metals (M), such as Li, Na, or K, in which the stoichiometry of MC_x was varied over a wide range of x values.[17] The yield deduced from the slope of the C/K ratio of the single-wall CNT salts against the C/K ratio of reagents varied from 50% to 80%. Similar assessments on BNNTs as a function of $M(BN)_{x/2}$ stoichiometry would be desirable to verify our theoretical observations. We note, however, that further analysis on solvation energy differences between EA in the gas phase and reduction potential in solution for nanotube systems is required for more rigorous comparison to experiments.[34]

Our finding that the EAs for small-diameter BNNTs are mostly positive suggests that using reduced BNNTs as intermediates for their further functionalization could be feasible and effective, similar to what has been observed for CNT.[16,17]

Binding Energies of Free Radicals with BNNTs: Neutral *vs* Reduced. The interactions between free radicals and the sidewalls of neutral and charged nanotubes are investigated through DFT calculations. Methyl ($^{\bullet}CH_3$), hydroxyl ($^{\bullet}OH$), and amino ($^{\bullet}NH_2$) radicals were selected as representative species of carbon-, oxygen-, nitrogen-centered radicals, respectively. We also consider reactions with nitrene radical ($^{\bullet}NH$), which has a free electron pair as well as two unpaired electrons, and nonradical ammonia (NH_3), with its one free electron pair.

The binding energy of radical molecules on the sidewall of a nanotube is defined as the difference between the total energy of the nanotube−radical complex and the sum of the energies of the separate individual species. The binding energies are calculated as follows:

$$E_b^n = E_{tot}(\mathrm{NT} + \mathrm{radical}) - E_{tot}(\mathrm{NT}) - E_{tot}(\mathrm{radical})$$

$$E_b^r = E_{tot}(\mathrm{NT}^- + \mathrm{radical}) - E_{tot}(\mathrm{NT}^-) - E_{tot}(\mathrm{radical})$$

TABLE 1. Binding Energies of Various Free Radicals ($^{\bullet}CH_3$, $^{\bullet}NH_2$, $^{\bullet}OH$, $^{\bullet}NH$) and NH_3 to the Sidewalls of Neutral and Charged CNTs and BNNTs and the Binding Energy Differences between the Neutral and Charged Systems, ΔE_b and $\Delta E_b^{\dagger}$, Where $\Delta E_b^{\dagger}$ Are the Results Obtained from Gaussian

neutral tubes	E_b^n (eV)	reduced tubes	E_b^r (eV)	ΔE_b (eV)	$\Delta E_b^{\dagger}$ (eV)
$B_{30}N_{30} + {}^{\bullet}CH_3$	0.06	$B_{30}N_{30}^- + {}^{\bullet}CH_3$	−2.86	2.91	4.14
$B_{30}N_{30} + {}^{\bullet}NH_2$	−0.64	$B_{30}N_{30}^- + {}^{\bullet}NH_2$	−3.54	2.89	4.26
$B_{30}N_{30} + {}^{\bullet}OH$	−1.36	$B_{30}N_{30}^- + {}^{\bullet}OH$	−4.70	3.34	5.00
$B_{30}N_{30} + {}^{\bullet}NH$	−2.34	$B_{30}N_{30}^- + {}^{\bullet}NH$	−3.26	0.93	2.41
$B_{30}N_{30} + NH_3$	−0.43	$B_{30}N_{30}^- + NH_3$	−0.60	0.17	
$C_{60} + {}^{\bullet}CH_3$	−1.01	$C_{60}^- + {}^{\bullet}CH_3$	−1.24	0.24	0.12
$C_{60} + {}^{\bullet}NH_2$	−1.01	$C_{60}^- + {}^{\bullet}NH_2$	−1.33	0.32	0.19
$C_{60} + {}^{\bullet}OH$	−1.63	$C_{60}^- + {}^{\bullet}OH$	−2.09	0.46	0.22
$C_{60} + {}^{\bullet}NH$	−3.14	$C_{60}^- + {}^{\bullet}NH$	−1.82	−1.32	−2.39
$C_{60} + NH_3$	−0.23	$C_{60}^- + NH_3$	−0.34	0.11	

for neutral and charged nanotubes, respectively. The total energy is calculated using the fully optimized geometry of corresponding reactants and products. In this study, reduced nanotubes are charged with a charge density of $\rho = -1/60$ (e/atom). In Table 1, we summarized the calculated binding energies, together with the binding energy differences between neutral and charged complexes, which are estimated by $\Delta E_b = E_b^n - E_b^r$. For all but one of the radical molecules considered here our DFT calculations predicted negative binding energies. For the neutral BNNT−CH_3 complex the reactants and product have almost identical enthalpy values (the enthalpy increases by only 0.06 eV upon binding). Such exothermic reactions indicate that the complex formations are energetically more stable with respect to the separated species; thus their functionalization is favorable. Note that binding occurs at B sites on BNNT surfaces.

Before reduction, CNTs demonstrate overall stronger binding affinities than BNNTs toward the radicals examined here. In particular, the reactivity of neutral BNNTs toward methyl radicals ($^{\bullet}CH_3$) is noticeably weaker than that of the neutral CNT. For both of the neutral nanotube species, reaction with the nitrene radical is predicted to be the most favorable of the radical reactions that were investigated. With the introduction of one extra electron per $N = 60$ atoms, the reduced BNNT is found to significantly improve its binding affinity toward all radical species, with changes in binding energies relative to the neutral nanotube reactions that are much larger in magnitude than those for the CNT. We benchmark our VASP calculation results against the results obtained by using a hybrid functional B3LYP and a 6-13G* basis set, which are presented as $\Delta E_b^{\dagger}$ in Table 1. Although $\Delta E_b^{\dagger}$ are found to be ∼1.5 eV higher than ΔE_b for most BNNT complexes, qualitatively similar trends have been observed in terms of binding energy increments from both calculations. We note that the goal of our current studies is to provide insights on experimental realization of reductive functionalization methods on BNNTs and to capture intrinsic and qualitative differences between the BNNT and CNT systems, rather than to estimate quantitatively accurate values of EAs and binding energies.

The fully optimized geometries of the BNNT complexes also suggest stronger binding affinity of the reduced BNNTs compared to the neutral BNNTs. The optimized configuration of the charged BNNT−CH_3 complex is depicted in Figure 3a, and the bond lengths and angles are presented in Figure 3b for neutral (left) and charged (right) complexes. For both cases, new B−C bonds are formed between a B atom on the BNNT network and the C atom in the methyl radical through rehybridization from sp^2 to sp^3. The sp^3 hybridization is more prominent for the charged complex, as indicated by the larger displacement of the B atom from the BN plane and more pronounced tetrahedral geometry for the methyl ligand. The N−B−N bond angles on the sidewall are decreased by up to ∼6.5° for the charged complex. The length of the B−C bond also appears shorter by 0.2 Å for the charged complex. All of these observations clearly support the stronger bond formation for the reduced BNNT.

The role of the excess electrons in the formation of the covalent bond is also investigated by examining the electron density distribution, particularly in close proximity to the newly formed B−C bonds. In Figure 3 we compare the total charge density of the neutral BNNT−CH_3 complex (c) to its charged counterpart (d) plotted at various isosurface levels (0.7, 1.0, and 1.7 e/Å^3, from left to right). At all of the charge densities we observe that more electron density accumulates in the B−C bond for the charged complex, which leads to its stronger bond formation. We also performed Bader charge analysis[35] and computed the charge difference, $\Delta q = q_C^r - q_C^n$, where q_C^r and q_C^n are the total charge on the C atom in $^{\bullet}CH_3$ from reduced and neutral complexes, respectively, which was found to be 0.47e. In contrast, for the CNT case, Δq was estimated to be 0.03e, which indicates that the extra electron is delocalized over the CNT surface and does not particularly contribute to the new C−C bond formation, resulting in only a small increase of their binding energy toward $^{\bullet}CH_3$ upon reduction. For BNNTs the valence electrons on tube surface are localized around N atoms (Figure 1b), and, therefore, the excess electrons likely fill the empty p orbitals of B atoms[36] and are able to form a strong covalent bond together with the unpaired electrons from the radical. The empty B atom sites, which serve as the localization sites for the excess electrons, make reductive functionalization of BNNTs an efficient route to achieve covalent chemistry on B sites.

Now we study the results for the formation of BNNT−NH_2 complexes. Unlike $^{\bullet}CH_3$, an $^{\bullet}NH_2$ radical possesses a lone pair of electrons in addition to the

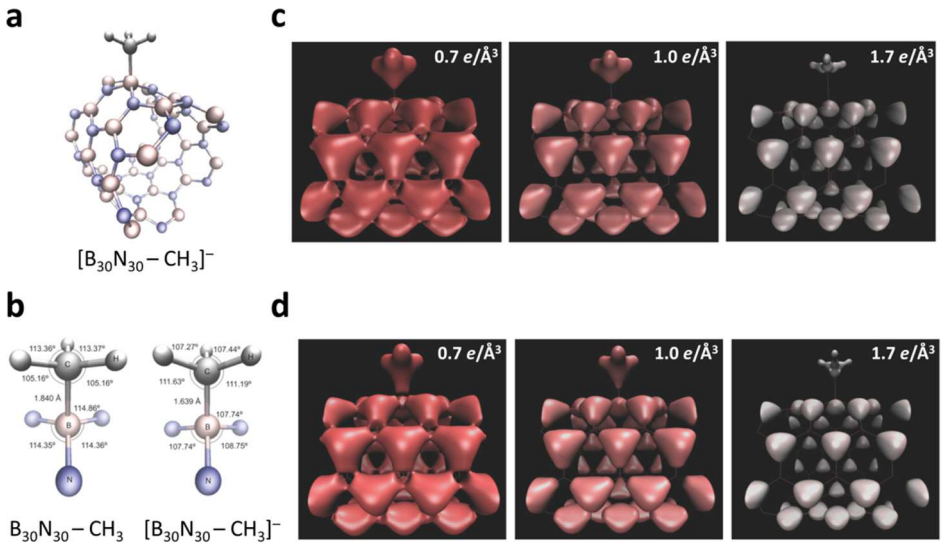

Figure 3. Optimized structure of a reduced (5,5) BNNT functionalized with $^{\bullet}CH_3$ (a); the bond lengths and angles for neutral (left) and charged (right) BNNT−CH_3 complexes (b); electron density distributions for neutral (c) and charged (d) BNNT−CH_3 complexes at various isovalues of the total valence charge density of 0.7, 1.0, and 1.7 e/Å^3 (from left to right).

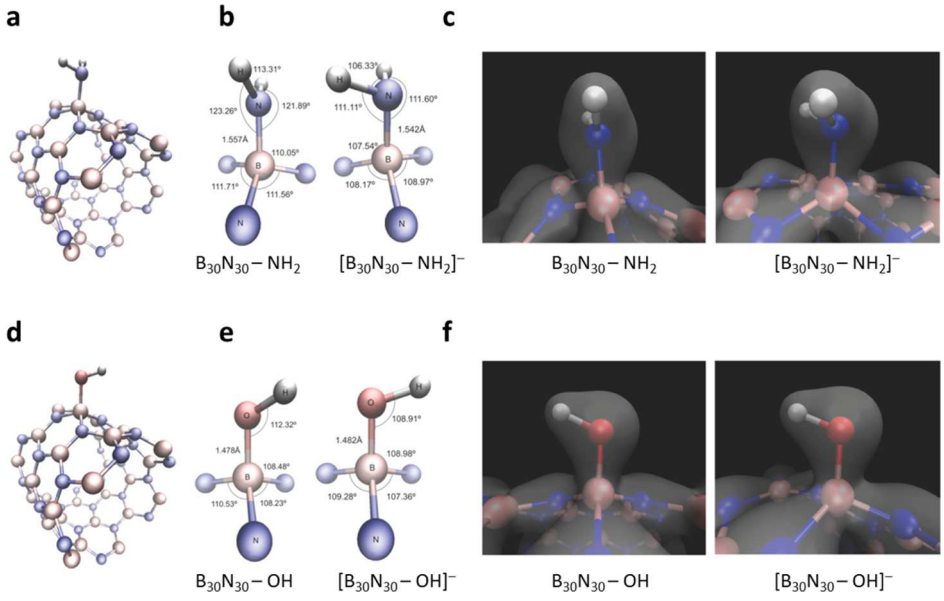

Figure 4. Optimized geometries and electron density distributions at the isosurface of 0.5 e/Å^3 in close proximity to the newly formed bonds for the complexes of BNNT−NH_2 in (a), (b), and (c) and BNNT−OH in (d), (e), and (f).

unpaired electron. The optimized binding geometry for the charged complex is illustrated in Figure 4a and b. Covalent bond formation between a B atom from the BNNT sidewall and the $^{\bullet}NH_2$ radical is exothermic for both the neutral and reduced BNNTs, with the charged BNNT exhibiting a much stronger binding to $^{\bullet}NH_2$ radical, as evidenced from the calculated binding energies of −0.64 and −3.54 eV, respectively. Optimized geometry of the charged BNNT−NH_2 complex predicts a pronounced trigonal pyramidal geometry, with the N atom of the NH_2 ligand at the apex, and B−N−H bond angles decreased by almost 10° from the largely planar NH_2 ligand of the neutral complex. This differing geometry originates from the existence of a pair of electrons on the NH_2 ligand for the charged complex. In the neutral BNNT case a pair of electrons in the $^{\bullet}NH_2$ radical is donated to form the B−N bond. When the nanotube is reduced, however, the additional electron from the BNNT surface is available to contribute to the B−N bond, leaving a pair of electrons remaining on the N atom of the ligand. The electron density isosurfaces shown in Figure 4c demonstrate the pronounced accumulation of charge density on the N atom of the ligand for the charged complex. This observation is also supported by the calculated Bader charge difference of $\Delta q = q^{r}_{N} - q^{n}_{N} = 0.50e$. The charge difference between neutral and charged CNT−NH_2 complexes is found to be $\Delta q = 0.06e$, which, again,

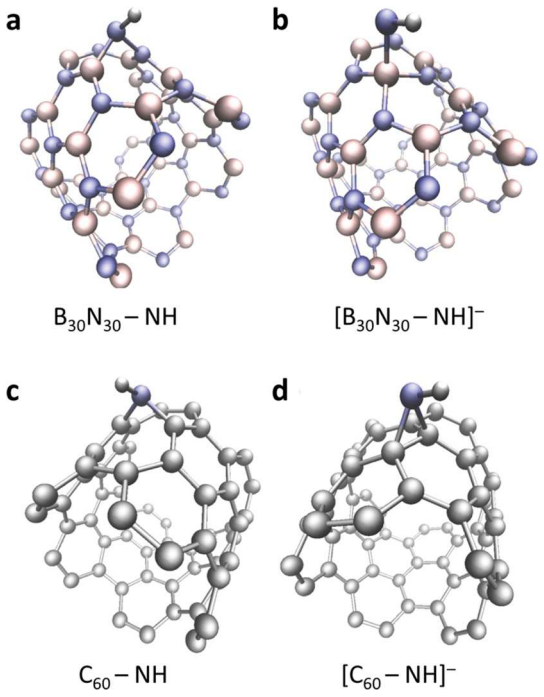

Figure 5. Optimized geometries of various nanotube−NH complexes: neutral BNNT−NH complex (a); charged BNNT−NH complex (b); neutral CNT−NH complex (c); charged CNT−NH complex (d).

supports the delocalization of extra electrons on the CNT tube surface.

We also studied the BNNT complex formation with an OH functional group. Hydroxyl radicals possess two lone pairs of electrons in addition to the unpaired electron. Similarly to the $^{\bullet}NH_2$ radical case, the binding of an $^{\bullet}OH$ radical to the neutral BNNT is energetically favorable, while reducing the BNNT results in significant enhancement of the binding affinity. In fact, the $^{\bullet}OH$ radical shows the greatest increase in binding energy of the species studied following reaction with a reduced nanotube, with a change of 3.34 eV relative to the neutral nanotube complex. The optimized geometries and charge density distributions of both the neutral and charged BNNT−OH complexes are shown in Figure 4d, e, and f, respectively. There are only small differences in geometry and electron density distribution between the two systems. In this case, the Bader analysis provides $\Delta q = q_O^r - q_O^n = 0.17e$. For CNT−OH complexes Δq is found to be negative, $-0.16e$. These relatively small differences are likely due to the strong electronegativity of the oxygen atom.

Recently, highly reactive nitrene radicals ($^{\bullet}NH$) have been used to covalently functionalize h-BN nanosheets.[14] Nitrene radicals possess one lone pair of electrons and *two* unpaired electrons in its triplet ground state. As shown in Figure 5a, the optimized geometry calculated for the neutral BNNT−NH complex exhibits a disruption of the nanotube network by breaking a B−N bond on the BNNT wall and creating new B−N and N−N bonds with the $^{\bullet}NH$ radical.[15] The binding energy of the neutral BNNT−NH complex is found to be the largest (−2.34 eV) of all that have been studied. The reduced BNNT forms a *radical anionic* complex with the $^{\bullet}NH$ radical through creation of a new B−N bond and without the disruption of the nanotube network. In contrast to the other systems studied, the charged BNNT−NH complex shows only a moderate improvement in binding affinity (0.93 eV) over its neutral counterpart. It is interesting to compare this result to the CNT−NH complex formation. The neutral CNT−NH complex is also found to be stable, with an enthalpy gain of 3.14 eV, and exhibits a similar bond topology to the neutral BNNT−NH complex, with two newly formed C−N bonds and a C−C bond breakage. However, the reduced CNT leads to formation of two new C−N bonds without involving C−C bond breakage on the CNT network. In this case the binding affinity of the CNT toward the $^{\bullet}NH$ radical decreases by 1.32 eV upon reduction and represents the only case studied in which the charged complex is less favored than the neutral complex. We note that the interaction of neutral BNNTs with the $^{\bullet}NH$ radical results in *nonradical* complexes with two unpaired electrons associated with two distinct bonds, while their charged counterparts form *radical anionic* complexes. In contrast, the neutral BNNT complexes formed with CH_3, OH, and NH_2 are *radical*, while their charged counterparts are *nonradical anionic*. This results in the small value of ΔE_b for NT−NH complexes. Utilization of reduced nanotubes for NH functionalization could still be advantageous over neutral ones because the hexagonal networks are preserved; thus the mechanical properties of the functionalized nanotubes could be retained close to those of pristine unfunctionalized tubes.

We also evaluated the binding energy for nanotube reactions with NH_3, the simplest amino functional group, as an example of nonradical molecules. The binding energies calculated here are consistent with previous works.[37,38] In this case, we have not observed any significant increments in binding energy for either BNNTs or CNTs upon reduction.

Covalent Alkylation of BNNTs Using 1-Bromohexane: Reduced *vs* Neutral BNNT. Here we briefly report experimental results of the covalent alkylation of BNNTs *via* reduction chemistry using 1-bromohexane as illustrated in Scheme 1. Neutral BNNTs were also reacted with 1-bromohexane under the same reaction conditions in order to investigate the key role of the reduction chemistry of BNNTs on their subsequent reactivity. We note that although the alkyl chain length of 1-bromohexane ($^{\bullet}(CH_2)_5CH_3$) is much longer than the smallest methyl radical ($^{\bullet}CH_3$) that we examined in our theoretical calculation, the effect of the alkyl chain on the chemical reactivity of radicals is considered to be negligible.[39]

Thermogravimetric (TG) analysis is widely used for the direct characterization of covalently functionalized

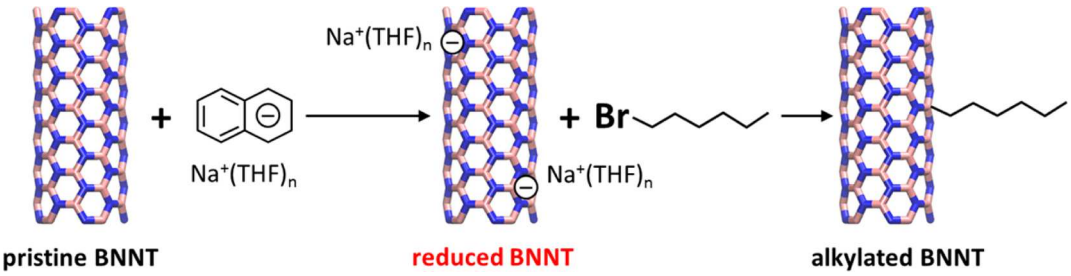

Scheme 1. Schematic illustration of the covalent alkylation of BNNTs *via* reduction chemistry using 1-bromohexane.

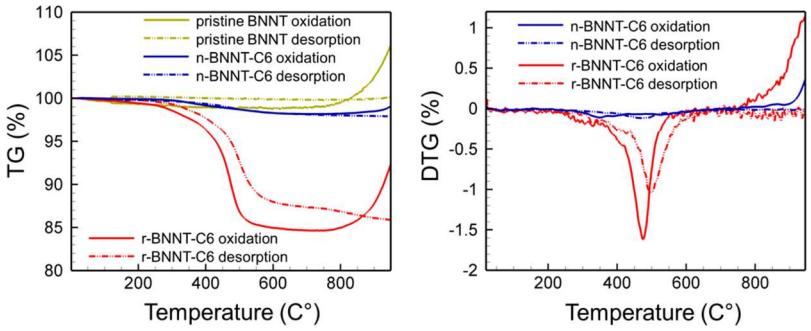

Figure 6. Thermogravimetric analyses of pristine and alkylated BNNT samples under desorption and oxidation conditions. "r-BNNT-C6" and "n-BNNT-C6" stand for the reaction products from the reactions of 1-bromohexane with reduced BNNTs and neutral BNNTs, respectively.

nanotubes.[19,40] Detachment or oxidation of the species covalently bonded to nanotube surfaces occurs at relatively low temperatures compared to the decomposition temperatures of the nanotubes themselves (*e.g.*, BNNTs are thermally stable to greater than 750 °C in air). Mass losses at such lower temperatures can be strong evidence of the presence of covalently bonded species on nanotube surfaces. The TG and DTG data of the pristine BNNTs and the samples from the reactions of the reduced and the neutral BNNTs with 1-bromohexane are shown in Figure 6. The pristine BNNTs exhibit almost no mass change for the entire temperature range in desorption and only slight weight gain in oxidation due to the thermal oxidation of BNNTs themselves into boron oxide above 750 °C. The baseline sample from the reaction of the neutral BNNTs with 1-bromohexane does not differ greatly from that of the pristine BNNTs, showing only small weight losses (1−2%) occurring between 350 and 500 °C (Figure 6b), possibly due to the removal of some organic residues remaining in the sample or to detachment or oxidation of alkyl chains grafted to the nanotube surface in the functionalization reaction. If we attribute it to the latter, the small magnitude of the mass change implies that there was minimal alkylation of the neutral BNNT surface. In contrast, large mass changes of about 12% in desorption and 14% in oxidation between 400 and 600 °C are observed for the sample from the reaction of the reduced BNNTs with 1-bromohexane, suggesting that a higher degree of functionalization was achieved and that the reactivity of BNNTs has been greatly improved by reduction.

Infrared (IR) absorption spectra of the pristine and functionalized samples are presented in Figure 7. The spectrum of the pristine BNNTs is composed of the in-plane B−N stretching and the out-of-plane B−N−B bending modes observed at 1383 and 806 cm^{-1}, respectively. The FTIR spectrum of the sample from the neutral BNNTs' reaction with 1-bromohexane is similar to that of the pristine BNNTs, except for a broadening of the BN stretching mode and the appearance of a weak band in the 3000−2800 cm^{-1} region attributable to C−H stretching modes. A broad peak appearing at 3200 cm^{-1} is due to surface moisture. The broadening toward higher frequency of the in-plane BN stretching modes at 1383 cm^{-1} is primarily attributable to covalent bonding to the nanotube surface disrupting the sp^2-bonding network, although it is also possible that adsorption of 1-bromohexane on the BNNT through van der Waals adhesion could contribute. A 10 cm^{-1} shift observed for the out-of-plane mode near 800 cm^{-1} for both of the reacted samples relative to the pristine BNNT can also be explained in this way. The spectrum of the sample from the reaction of the reduced BNNTs with 1-bromohexane exhibits similar C−H stretching signatures as well as the appearance of a new peak at 1153 cm^{-1}, which corresponds to B−C stretching. The appearance of this peak is indicative of there being covalent binding of the alkyl chains to BNNT surfaces and evidence of enhanced reactivity of reduced BNNTs. This observation is also consistent with our calculation result that bonding occurs at B sites on BNNT surfaces. The in-plane B−N stretching mode has also shifted by 4 cm^{-1} to

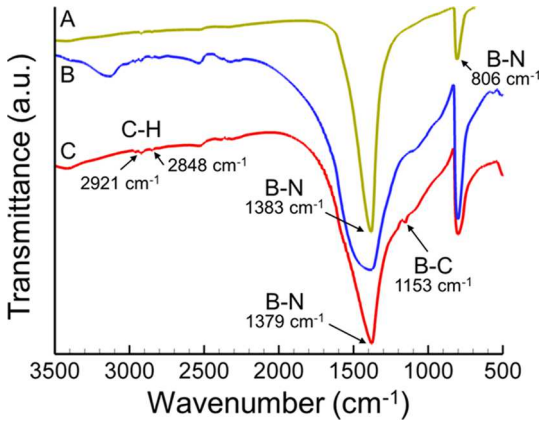

Figure 7. FTIR spectra of pristine BNNTs (a), the reaction product from neutral BNNTs with 1-bromohexane (b), and the reaction product from reduced BNNTs with 1-bromohexane (c).

1379 cm^{-1} for this sample. This observation also supports our theoretical prediction that structural deformation of the BN lattices occurs through the rehybridization from sp^2 to sp^3 at the newly formed B−C bond sites.

CONCLUSIONS

Boron nitride nanotubes have inherently low chemical reactivity, so the development of effective protocols for their surface modification is essential for their real-world applications. Here we have shown using DFT simulations that covalent functionalization *via* reduction chemistry is a highly effective route for the surface modification of BNNTs. Our theoretical investigations have found that, upon reduction, the chemical reactivity of BNNTs toward radical molecules is drastically increased (*e.g.*, 5.5-fold enhancement in reactivity with the $^{\bullet}NH_2$ radical over their neutral counterparts). Carbon nanotubes did not show the same degree of improved reactivity, implying that reduced BNNTs should be a more effective means of achieving functionalization than reduced CNTs. The calculated total charge differences reveal that the localization of the excess electrons in the empty B-centered orbitals of the BNNTs plays an important role in the enhanced reactivity by promoting covalent bond formation with the unpaired electrons in the radicals. This was not observed for reduced CNTs because the excess electrons were delocalized over the nanotube. We also observed that the reactivity enhancement of reduced BNNTs is influenced by the detailed electronic configurations of the radicals, such as singlet or triplet states and the existence of electron lone pairs. In support of our theoretical findings, we experimentally investigated the covalent alkylation of BNNTs *via* reduction chemistry using 1-bromohexane. The TG and IR measurements clearly confirmed the significant increase in reactivity of reduced BNNTs toward covalent alkylation compared to neutral nanotubes, in full agreement with our theoretical studies. These new findings will provide useful guidelines for the development of effective covalent functionalization schemes for BNNTs *via* reduction reactions. We conclude that the investigation on how electronic[41,42] or mechanical properties of BNNTs would be changed or controlled upon their covalent functionalization with various functional groups is worth future studies in order to find out the distinct applications of BNNTs, such as polymer nanocomposites, nonconventional electronics, or biomaterials.[43]

MATERIALS AND METHODS

Density Functional Theory Simulations. We performed the DFT calculations within a framework of generalized gradient approximation (GGA) with the Perdew−Burke−Ernzehof (PBE) exchange−correlation functional[44] by using the project augmented wave (PAW) method as implemented in the Vienna Ab Initio Simulation Package (VASP).[45] The basis set consists of plane waves with a cutoff energy of 600 eV. To implement charged systems with excess electrons, a neutralizing background charge was applied. For open-shell radicals, the spin-unrestricted (polarized) calculations were performed. The geometrically optimized configurations of isolated nanotubes, free radicals, and the nanotube−radical complexes were obtained by relaxing all the atomic coordinates using the conjugated gradient algorithm, until the residual force became less than 0.01 eV/Å.

EA calculations were carried out with supercells of armchair [(5,5) and (10,10)] and zigzag [(5,0) and (10,0] nanotubes for both C and BN systems. We used rectangular model cells, whose $x-y$ dimensions perpendicular to the tube axis were 30 Å, chosen sufficiently large enough to avoid the tube−tube interactions from adjacent unit cells. The supercell length in the z direction is varied to explore different charge densities on the tube surfaces, for instance, from 1 up to 4 unit cells. The lengths of one unit cell were 2.46 and 4.26 Å for armchair and zigzag CNTs, respectively, and 2.49 and 4.32 Å for armchair and zigzag BNNTs, respectively. In all the calculations, periodic boundary conditions were imposed along the tube axis to simulate infinitely long nanotube systems. The integration over the Brillouin zone was performed using the Monhhorst−Pack method with $1 \times 1 \times \alpha$ k-point grids, where α is chosen as 12, 6, 4, and 3, for 1, 2, 3, and 4 unit cells, respectively. For the benchmark, we also calculated the EA of fullerenes, using a supercell of $20 \times 20 \times 20$ $Å^3$ with a $1 \times 1 \times 1$ k-point grid.

To compute binding energies of various free radicals toward the sidewall of nanotubes, we used (5,5) nanotube supercells containing 3 unit cells with $N = 60$ atoms/cell, where N is the number of C atoms (for CNTs) or B and N atoms (for BNNTs), to avoid any unphysical interactions between periodic images of radical molecules. The supercell dimensions are $30 \times 30 \times 7.38$ $Å^3$ and $30 \times 30 \times 7.48$ $Å^3$ for CNTs and BNNTs, respectively, and Monhhorst−Pack k-points with $1 \times 1 \times 4$ were used for both cases. To benchmark our calculations with VASP, optimized geometries of NT complexes and binding energies were also calculated using the B3LYP hybrid functional and a 6-31G* basis set with Gaussian.[46]

Synthesis and Purification of Boron Nitride Nanotubes. Raw pristine BNNTs were synthesized by the newly developed hydrogen-assisted BNNT synthesis (HABS) method.[3] Hexagonal boron nitride powder (99.5%, av 70 nm, MK-hBN-N70, M K Impex Corp.) was employed as feedstock and dried at 100 °C overnight before use. The h-BN powder was injected into an induction thermal plasma operated at 50 kW plate power by using 3 slpm

of Ar carrier gas. The feed rate was maintained at 0.5−1.0 g/min. The plasma was generated by a commercial induction plasma torch (Tekna PS-50, Tekna Systems, Inc.) composed of a five-turn coil and a ceramic tube with an internal diameter of 50 mm. Pure Ar gas (30 slpm) was injected into the central region of the torch for stable plasma generation, and a ternary gas mixture of Ar (45 slpm), N_2 (55 slpm), and H_2 (20 slpm) was introduced along the ceramic tube wall, offering further plasma stabilization and chemical reactions. The produced raw BNNT materials contained amorphous boron and h-BN flake impurities and were purified through a scalable, nondestructive postprocessing protocol involving a combination of thermal treatments similar to the one reported by Chen *et al.*[47] and solvent washing.

Reduction of Boron Nitride Nanotubes. We employed a similar approach reported for CNTs.[16,19,48] To reduce BNNTs, the purified nanotubes (80 mg) were dispersed in 100 mL of dry THF in a 250 mL Schlenk round-bottom flask using bath sonication, and then the preprepared sodium naphthalide green solution (745 mg of Na, 4.3 g of naphthalene in 120 mL of THF) was added to the BNNT suspension under an argon atmosphere. The mixture was magnetically stirred for 24 h.

Alkylation of Boron Nitride Nanotubes with 1-Bromohexane. For the *in situ* alkylation to the surfaces of the reduced BNNTs, 1-bromohexane (3 mL, Sigma-Aldrich) was added to the above suspension, followed by an additional 48 h of stirring at room temperature. The reaction mixture was then diluted with MeOH and distilled water. After settling of the mixture for a few minutes, the top solution was discarded and the bottom precipitate was refilled with THF, MeOH, and H_2O in turn. After two settling and discarding cycles, the bottom precipitate was collected through a polycarbonate membrane (PC, pore size: >20 μm,). The collected precipitate was further washed with distilled water and MeOH a few times in turn and dried in air under vacuum and then dried in an oven at 130 °C for 2 days. For comparison, the covalent alkylation was attempted using neutral BNNTs with the same approach.

Characterization of Boron Nitride Nanotube Samples. The BNNT samples were characterized by TGA (Netzsch TG 209 F1 Iris) and FTIR (Nicolet 6700 FT-IR). TGA data were obtained by heating a ~10 mg sample under argon (desorption) or air (oxidation) atmosphere to 950 °C at a rate of 10 °C/min. In the FT-IR analysis, samples were prepared by grinding with KBr powder and pressing into disc pellets.

Conflict of Interest: The authors declare no competing financial interest.

Acknowledgment. This work was supported by the NRC Security Materials Technology Program. The authors express their thanks to Malgorzata Daroszewska and Michael Barns for the TGA measurements and to Mark Plunkett for supporting synthesis of the BNNT materials. The authors also thank Dr. Andrew Johnston for his careful reading of the manuscript.

REFERENCES AND NOTES

1. Chopra, N. G.; Luyken, R. J.; Cherrey, K.; Crespi, V. H.; Cohen, M. L.; Louie, S. G.; Zettl, A. Boron Nitride Nanotubes. *Science* **1995**, *269*, 966–967.
2. Golberg, D.; Bando, Y.; Huang, Y.; Terao, T.; Mitome, M.; Tang, C.; Zhi, C. Boron Nitride Nanotubes and Nanosheets. *ACS Nano* **2010**, *4*, 2979–2993.
3. Kim, K. S.; Kingston, C. T.; Hrdina, A.; Jakubinek, M. B.; Guan, J.; Plunkett, M.; Simard, B. Hydrogen-Catalyzed, Pilot-Scale Production of Small-Diameter Boron Nitride Nanotubes and Their Macroscopic Assemblies. *ACS Nano* **2014**, *8*, 6211–6220.
4. Fathalizadeh, A.; Pham, T.; Mickelson, W.; Zettl, A. Scaled Synthesis of Boron Nitride Nanotubes, Nanoribbons, and Nanococoons Using Direct Feedstock Injection into an Extended-Pressure, Inductively-Coupled Thermal Plasma. *Nano Lett.* **2014**, *14*, 4881–4886.
5. Smith, M. W.; Jordan, K. C.; Park, C.; Kim, J.-W.; Lillehei, P. T.; Crooks, R.; Harrison, J. S. Very Long Single- and Few-Walled Boron Nitride Nanotubes *via* the Pressurized Vapor/Condenser Method. *Nanotechnology* **2009**, *20*, 505604.
6. Kim, K. S.; Jakubinek, M. B.; Martinez-Rubi, Y.; Ashrafi, B.; Guan, J.; O'Neill, K.; Plunkett, M.; Hrdina, A.; Lin, S.; Denommee, S.; *et al.* Polymer Nanocomposites from Free-standing, Macroscopic Boron Nitride Nanotube Assemblies. *RSC Adv.* **2015**, *5*, 41186–41192.
7. Xie, S.-Y.; Wang, W.; Fernando, K. A. S.; Wang, W.; Lin, Y.; Sun, Y.-P. Solubilization of Boron Nitride Nanotubes. *Chem. Commun.* **2005**, 3670–3672.
8. Pal, S.; Vivekchand, S. R. C.; Govindaraj, A.; Rao, C. N. R. Functionalization and Solubilization of BN Nanotubes by Interaction with Lewis Bases. *J. Mater. Chem.* **2007**, *17*, 450–452.
9. Zhi, C.; Bando, Y.; Tang, C.; Sekiguchi, T.; Golberg, D. Perfectly Dissolved Boron Nitride Nanotubes Due to Polymer Wrapping. *J. Am. Chem. Soc.* **2005**, *127*, 15996–15997.
10. Gao, Z.; Zhi, C.; Bando, Y.; Golberg, D.; Serizawa, T. Isolation of Individual Boron Nitride Nanotubes *via* Peptide Wrapping. *J. Am. Chem. Soc.* **2010**, *132*, 4976–4977.
11. Velayudham, S.; Lee, C. H.; Xie, M.; Blair, D.; Bauman, N.; Yap, Y. K.; Green, S. A.; Liu, H. Noncovalent Functionalization of Boron Nitride Nanotubes with Poly(*p*-phenylene-ethynylene)s and Polythiophene. *ACS Appl. Mater. Interfaces* **2010**, *2*, 104–110.
12. Ciofani, G.; Genchi, G. G.; Liakos, I.; Athanassiou, A.; Dinucci, D.; Chiellini, F.; Mattoli, V. A. Simple Approach to Covalent Functionalization of Boron Nitride Nanotubes. *J. Colloid Interface Sci.* **2012**, *374*, 308–314.
13. Sainsbury, T.; Satti, A.; May, P.; Wang, Z.; McGovern, I.; Gun'ko, Y. K.; Coleman, J. N. Oxygen Radical Functionalization of Boron Nitride Nanosheets. *J. Am. Chem. Soc.* **2012**, *134*, 18758–18771.
14. Sainsbury, T.; Satti, A.; May, P.; O'Neill, A.; Nicolosi, V.; Gun'ko, Y. K.; Coleman, J. N. Covalently Functionalized Hexagonal Boron Nitride Nanosheets by Nitrene Addition. *Chem.—Eur. J.* **2012**, *18*, 10808–10812.
15. Sainsbury, T.; O'Neill, A.; Passarelli, M. K.; Seraffon, M.; Gohil, D.; Gnaniah, S.; Sepncer, S. J.; Rae, A.; Coleman, J. N. Dibromocarbene Functionalization of Boron Nitride Nanosheets: Toward Band Gap Manipulation and Nanocomposite Applications. *Chem. Mater.* **2014**, *26*, 7039–7050.
16. Penicaud, A.; Poulin, P.; Derre, A.; Anglaret, E.; Petit, P. Spontaneous Dissolution of a Single-Wall Carbon Nanotube Salt. *J. Am. Chem. Soc.* **2005**, *127*, 8–9.
17. Voiry, D.; Roubeau, O.; Penicaud, A. Stoichiometric Control of Single Walled Carbon Nanotubes Functionalization. *J. Mater. Chem.* **2010**, *20*, 4385–4391.
18. Martinez-Rubi, Y.; Guan, J.; Lin, S.; Scriver, C.; Sturgeon, R. E.; Simard, B. Rapid and Controllable Covalent Functionalization of Single-Walled Carbon Nanotubes at Room Temperature. *Chem. Commun.* **2007**, 5146–5148.
19. Guan, J.; Martinez-Rubi, Y.; Denommee, S.; Ruth, D.; Kingston, C. T.; Daroszewska, M.; Barnes, M.; Simard, B. About the Solubility of Reduced SWCNT in DMSO. *Nanotechnology* **2009**, *20*, 245701.
20. Liang, F.; Sadana, A. K.; Peera, A.; Chattopadhyay, J.; Gu, Z.; Hauge, R. H.; Billups, W. E. A Convenient Route to Functionalized Carbon Nanotubes. *Nano Lett.* **2004**, *4*, 1257–1260.
21. Chattopadhyay, J.; Chakraborty, S.; Mukherjee, A.; Wang, R.; Engel, P. S.; Billups, W. E. SET Mechanism in the Functionalization of Single-Walled Carbon Nanotubes. *J. Phys. Chem. C* **2007**, *111*, 17928–17932.
22. Fogden, S.; Howard, C. A.; Heenan, R. K.; Skipper, N. T.; Shaffer, M. S. P. Scalable Method for the Reductive Dissolution, Purification, and Separation of Single-Walled Carbon Nanotubes. *ACS Nano* **2012**, *6*, 54–62.
23. Jiang, C.; Saha, A.; Xiang, C.; Young, C. C.; Tour, J. M.; Pasquali, M.; Marti, A. A. Increased Solubility, Liquid-Crystalline Phase, and Selective Functionalization of Single-Walled Carbon Nanotube Polyelectrolyte Dispersions. *ACS Nano* **2013**, *7*, 4503–4510.
24. Hof, F.; Bosch, S.; Eigler, S.; Hauke, F.; Hirsch, A. New Basic Insight into Reductive Functionalization Sequences of Single Walled Carbon Nanotubes (SWCNTs). *J. Am. Chem. Soc.* **2013**, *135*, 18385–18395.

25. Hof, F.; Hauke, F.; Hirsch, A. Brominated Single Walled Carbon Nanotubes as Versatile Precursors for Covalent Sidewall Functionalization. *Chem. Commun.* **2014**, *50*, 6582–6584.
26. Ostfeld, A. E.; Catheline, A.; Ligsay, K.; Kim, K.-C.; Chen, Z.; Facchetti, A.; Fogden, S.; Arias, A. C. Single-Walled Carbon Nanotube Transparent Conductive Films Fabricated by Reductive Dissolution and Spray Coating for Organic Photovoltaics. *Appl. Phys. Lett.* **2014**, *105*, 253301.
27. Jiang, C.; Saha, A.; Marti, A. A. Carbon Nanotubides: An Alternative for Dispersion, Functionalization and Composites Fabrication. *Nanoscale* **2015**, *7*, 15037–15045.
28. Berseth, P. A.; Harter, A. G.; Zidan, R.; Blomqvist, A.; Araujo, C. M.; Scheicher, R. H.; Ahuja, R.; Jena, P. Carbon Nanomaterials as Catalysts for Hydrogen Uptake and Release in $NaAlH_4$. *Nano Lett.* **2009**, *9*, 1501–1505.
29. Buonocore, F.; Trani, F.; Matteo, A. D.; Cantele, G.; Iadonisi, G. *Ab Initio* Calculations of Electron Affinity and Ionization Potential of Carbon Nanotubes. *Nanotechnology* **2008**, *19*, 025711.
30. Luo, J.; Peng, L.-M; Xue, Z. Q.; Wu, J. L. Density-Functional-Theory Calculations of Charged Single-Walled Carbon Nanotubes. *Phys. Rev. B: Condens. Matter Mater. Phys.* **2002**, *66*, 115415.
31. Rienstra-Kiracofe, J. C.; Tschumper, G. S.; Schaefer, H. F., III. Atomic and Molecular Electron Affinities: Photoelectron Experiments and Theoretical Computations. *Chem. Rev.* **2002**, *102*, 231–282.
32. Wang, X. B.; Ding, C. F.; Wang, L. S. High Resolution Photoelectron Spectroscopy of C_{60}^-. *J. Chem. Phys.* **1999**, *110*, 8217–8220.
33. Haddon, R. C. Chemistry of the Fullerenes: The Manifestation of Strain in a Class of Continuous Aromatic Molecules. *Science* **1993**, *261*, 1545–1550.
34. Ruoff, R. S.; Kadish, K. M.; Boulas, P.; Chen, E. C. M. Relationship between the Electron Affinities and Half-Wave Reduction Potentials of Fullerenes, Aromatic Hydrocarbons, and Metal Complexes. *J. Phys. Chem.* **1995**, *99*, 8843–8850.
35. Tang, W.; Sanville, E.; Henkelman, G. A Grid-Based Bader Analysis Algorithm without Lattice Bias. *J. Phys.: Condens. Matter* **2009**, *21*, 084204.
36. Sun, Q.; Li, Z.; Searles, D. J.; Chen, Y.; Lu, G.; Du, A. Charge-Controlled Switchable CO_2 Capture on Boron Nitride Nanomaterials. *J. Am. Chem. Soc.* **2014**, *135*, 8246–8253.
37. Wu, X.; An, W.; Zeng, X. C. Chemical Functionalization of Boron-Nitride Nanotubes with NH_3 and Amino Functional Groups. *J. Am. Chem. Soc.* **2006**, *128*, 12001–12006.
38. Li, Y.; Zhou, Z.; Zhao, J. Transformation from Chemisorption to Physisorption with Tube Diameter and Gas Concentration: Computational Studies on NH_3 Adsorption in BN Nanotubes. *J. Chem. Phys.* **2007**, *127*, 184705.
39. Denis, P. A. Interaction Between Alkyl Radicals and Single Wall Carbon Nanotubes. *J. Comput. Chem.* **2012**, *33*, 1511–1516.
40. Kingston, C. T.; Martinez-Rubi, Y.; Guan, J.; Barnes, M.; Scriver, C.; Sturgeon, R. E.; Simard, B. Coupled Thermogravimetry, Mass Spectrometry, and Infrared Spectroscopy for Quantification of Surface Functionality on Single-Walled Carbon Nanotubes. *Anal. Bioanal. Chem.* **2010**, *396*, 1037–1044.
41. Zhi, C.; Bando, Y.; Tang, C.; Golberg, D. Engineering of Electronic Structure of Boron-Nitride Nanotubes by Covalent Functionalization. *Phys. Rev. B: Condens. Matter Mater. Phys.* **2006**, *74*, 153413.
42. Cao, F.; Ren, W.; Ji, Y.-M.; Zhao, C. The Structural and Electronic Properties of Amine-Functionalized Boron Nitride Nanotubes *via* Ammonia Plasmas: A Density Functional Theory Study. *Nanotechnology* **2009**, *20*, 145703.
43. Fernandez-Yague, M. A.; Larranaga, A.; Gladkovskaya, O.; Stanley, A.; Tadayyon, G.; Guo, Y.; Sarasua, J.-R.; Tofail, S. A. M.; Zeugolis, D. I.; Pandit, A.; *et al.* Effects of Polydopamine Functionalization on Boron Nitride Nanotube Dispersion and Cytocompatibility. *Bioconjugate Chem.* **2015**, *26*, 2025–2037.
44. Perdew, J. P.; Burke, K.; Ernzerhof, M. Generalized Gradient Approximation Made Simple. *Phys. Rev. Lett.* **1996**, *77*, 3865–3868.
45. Kresse, G.; Furthmüller, J. Efficient Iterative Schemes for *Ab Initio* Total-Energy Calculations Using a Plane-Wave Basis Set. *Phys. Rev. B: Condens. Matter Mater. Phys.* **1996**, *54*, 11169–11186.
46. Frisch, M. J.; Trucks, G. W.; Schlegel, H. B.; Scuseria, G. E.; Robb, M. A.; Cheeseman, J. R.; Zakrzewski, V. G.; Montgomery Jr., J. A.; Stratmann, R. E.; Burant, J. C.; *et al. Gaussian 98*; Gaussian, Inc.: Pittsburgh, PA, 1998.
47. Chen, H.; Chen, Y.; Yu, J.; Williams, J. S. Purification of Boron Nitride Nanotubes. *Chem. Phys. Lett.* **2006**, *425*, 315–319.
48. Najafi, E.; Wang, J.; Hitchcock, A. P.; Guan, J. W.; Denommee, S.; Simard, B. Characterization of Single-Walled Carbon Nanotubes by Scanning Transmission X-ray Spectromicroscopy: Purification, Order and Dodecyl Functionalization. *J. Am. Chem. Soc.* **2010**, *132*, 9020–9029.